

A Fast Approximation for Seismic Inverse Modeling: Adaptive Spatial Resampling

Cheolkyun Jeong¹  · Tapan Mukerji¹ ·
Gregoire Mariethoz²

Received: 9 August 2016 / Accepted: 14 June 2017
© International Association for Mathematical Geosciences 2017

Abstract Seismic inverse modeling, which transforms appropriately processed geophysical data into the physical properties of the Earth, is an essential process for reservoir characterization. This paper proposes a work flow based on a Markov chain Monte Carlo method consistent with geology, well-logs, seismic data, and rock-physics information. It uses direct sampling as a multiple-point geostatistical method for generating realizations from the prior distribution, and Metropolis sampling with adaptive spatial resampling to perform an approximate sampling from the posterior distribution, conditioned to the geophysical data. Because it can assess important uncertainties, sampling is a more general approach than just finding the most likely model. However, since rejection sampling requires a large number of evaluations for generating the posterior distribution, it is inefficient and not suitable for reservoir modeling. Metropolis sampling is able to perform an equivalent sampling by forming a Markov chain. The iterative spatial resampling algorithm perturbs realizations of a spatially dependent variable, while preserving its spatial structure by conditioning to subset points. However, in most practical applications, when the subset conditioning points are selected at random, it can get stuck for a very long time in a non-optimal local minimum. In this paper it is demonstrated that adaptive subset sampling improves the efficiency of iterative spatial resampling. Depending on the acceptance/rejection criteria, it is possi-

✉ Cheolkyun Jeong
cjeong@slb.com

Tapan Mukerji
mukerji@stanford.edu

Gregoire Mariethoz
Gregoire.Mariethoz@unil.ch

¹ Department of Energy Resources Engineering, Stanford University, Stanford, CA 94305, USA

² Institute of Earth Surface Dynamics, University of Lausanne, Lausanne, Switzerland

ble to obtain a chain of geostatistical realizations aimed at characterizing the posterior distribution with Metropolis sampling. The validity and applicability of the proposed method are illustrated by results for seismic lithofacies inversion on the Stanford VI synthetic test sets.

Keywords Seismic inverse modeling · McMC · Metropolis sampling · Iterative spatial sampling · Adaptive spatial sampling

1 Introduction

Seismic data play a key role in reducing uncertainty when predicting rocks and fluids away from well control points. However, in real applications it is nearly impossible to find a unique relationship between seismic responses and reservoir properties. Seismic measurements are noisy and have larger vertical scales of resolution than well data. Moreover, the relationships are non-unique due to the limited frequency of seismic waves, the forward modeling simplifications, and the natural heterogeneity of the subsurface geology.

Statistical rock physics accounts for some of the uncertainty using multi-variate stochastic relations between elastic parameters and reservoir properties (Mukerji et al. 2001a, b; Avseth et al. 2005). Many different workflows have been suggested to combine rock physics and geostatistical methods in seismic inversion. Bosch et al. (2010) classified these approaches into two groups: the sequential or cascaded approach, and the joint or simultaneous workflow in a Bayesian formulation. Traditional sequential or cascaded approaches (Dubrule 2003; Doyen 2007) start by transforming elastic properties into statistical classification properties (probability maps), and use them as soft data for geostatistical simulation. The joint or simultaneous workflows account for the elastic parameters and the reservoir properties together, and provide combined uncertainties. These Bayesian workflows include rock-physics relations to link reservoir properties and elastic properties, and geostatistical models to provide geologically consistent prior models. Forward-modeled synthetic data are compared with obtained seismic data to calculate the likelihood, and the final solutions are posterior models consistent with the expected geology, well data, and seismic data.

Eidsvik et al. (2004) formulated a simultaneous inversion using a Bayesian network model, and incorporated the spatial continuity of priors in a Markov random-field model. Larsen et al. (2006) incorporated vertical spatial correlation using a Markov-chain model, while Ulvmoen and Omre (2010) applied the Markov chain model to lithology/fluid inversion in a Bayesian framework. Bachrach (2006) combined a Markov chain Monte Carlo (McMC) with stochastic rock physics modeling for joint estimation of porosity and saturation. Contreras et al. (2005) suggested a joint stochastic inversion of well logs and three-dimensional pre-stack seismic data based on McMC updates. Gonzalez et al. (2008) combined multiple point geostatistics (MPS) and rock physics for seismic inversion. They generated multiple realizations of reservoir facies and saturations, conditioned to seismic and well data. MPS is used to characterize the geologic prior information, while statistical rock physics links reservoir properties to elastic properties. Thus, their method provides multiple realizations, all consistent with

the expected geology, well-logs, seismic data, and local rock-physics transformations. However, this work flow does not produce samples of the full posterior probability density function (PDF), though it does multiple optimized models around the mode of the posterior. The SIMPAT MPS algorithm ([Arpat 2005](#)) was also inefficient for application to the three-dimensional and complicated actual field cases. Among posterior sampling methods, rejection sampler ([Tarantola 2005](#)) is a classic method to sample the posterior PDF. However, since it requires a large number of evaluations of the forward model, rejection sampling is inefficient. Therefore, a key issue is how to generate prior models and how to find the posterior models that honor both spatial constraints and seismic data, given limited computation time and cost.

In this paper, the authors propose an McMC workflow consistent with geology, well-logs, seismic data, and rock-physics information. According to the classification of [Bosch et al. \(2010\)](#), the proposed Markov chain work flow follows the simultaneous seismic inversion. The work flow uses direct sampling (DS), a multiple-point geostatistical method ([Mariethoz et al. 2010a, b](#)), for generating realizations from the prior distribution, and the Metropolis algorithm with adaptive spatial resampling (M-ASR) for approximate sampling from the posterior distribution, conditioned to the geophysical data. Since conventional MPS algorithms, such as SNESIM or SIMPAT, store all data events from the training image ([Strebelle and Journel 2001; Arpat 2005](#)), the computational cost is dramatically increased according to the size of the template and the number of facies. The DS algorithm directly samples the training image for any given data event, without storing all the patterns in a database. The principle of the method is that for each simulated node, the training image is randomly scanned for a given conditional data event. The value of the central node of the first matching data event is then used for simulation because it corresponds to a conditional sample. This simulation method is very lightweight in terms of memory usage, CPU efficient, flexible, and able to reproduce the structures of complex training images and deal with a range of non-stationary problems. Since DS is a fast and efficient pixel-based MPS technique, it is a good pair with the M-ASR method, which uses promising points for the next model generation. However, the strength of M-ASR is that it is not specific to DS but could be associated with any MPS algorithms such as SNESIM, DISPAT ([Honarkah and Caers 2012](#)), or CCSIM ([Tahmasebi et al. 2012](#)).

The McMC algorithm also perturbs realizations of a spatially dependent variable while preserving its spatial structure. Iterative spatial resampling (ISR) and adaptive spatial resampling (ASR) use the method as a transition kernel to produce a Markov chain of geostatistical realizations. These realizations are then used in a forward seismic model to compute the predicted data, which are compared to the observed data. Depending on the acceptance/rejection criterion in the Markov process, it is possible to obtain a chain of realizations aimed at characterizing the posterior distribution with Metropolis sampling. The proposed workflow is shown in Fig. 1. The important difference between ISR and ASR is that ASR adaptively samples a subset of points from the previously accepted model instead of using random selection. In most practical applications it is observed ISR chains get stuck for a long time in a certain stage, since the randomly selected unpromising points are iteratively used as conditioning points for model generation in the next step.

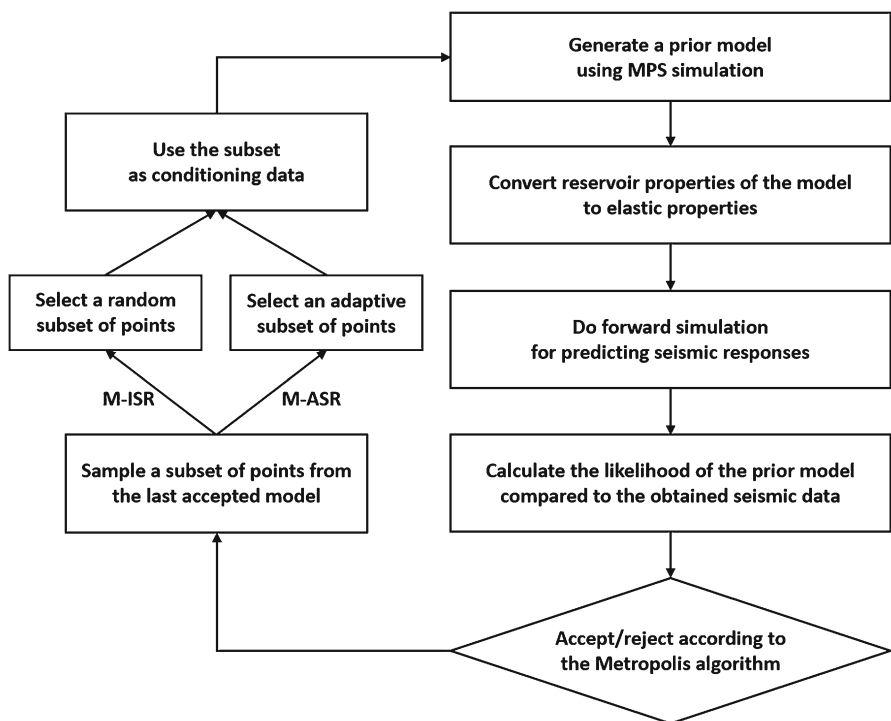


Fig. 1 A flowchart of the McMC process with the Metropolis sampler; in the resampling step for selecting conditioning points, the proposed M-ASR algorithm adaptively resamples a subset from the last accepted model instead of the random selection in ISR

Accordingly, in this paper the authors propose adaptive spatial resampling as a fast and approximate sampler for improving the efficiency of ISR, and demonstrate how it can be applied to seismic inversion. The proposed method is demonstrated on a set of synthetic test cases.

2 Methodology

2.1 Seismic Inverse Modeling in a Bayesian Framework

The transformation of geophysical data into reservoir properties can be posed as an inference problem involving the updating of prior knowledge with newly available data (Tarantola 1987, 2005). Following Bayes' rule, it can be expressed as

$$P_{\text{post}}(m) = c P_{\text{prior}}(m) P_{\text{data}}(d_{\text{obs}} - g(m)), \quad (1)$$

where $P_{\text{post}}(m)$ is the posterior probability density and $P_{\text{prior}}(m)$ is the a priori probability density. In Eq. (1), c is a normalizing constant, and m is the earth model parameter configuration. The expression $P_{\text{data}}(d_{\text{obs}} - g(m))$ is the likelihood func-

tion; it depends on the observations d_{obs} and their uncertainty, and the forward modeling operator g that maps the model space into the data space. The solutions of a given inverse problem are the set of earth-model configurations that, when forward-modeled into synthetic data, match the real data within some tolerance ([Bosch et al. 2010](#)).

[Bosch et al. \(2004\)](#) decomposed the model space into reservoir parameters (facies, porosity, etc.) and elastic parameters (seismic velocity and density), so the joint prior probability can be written as

$$P_{\text{prior}}(m_{\text{res}}, m_{\text{elas}}) = P_{\text{prior}}(m_{\text{res}}) P_{\text{prior}}(m_{\text{elas}}|m_{\text{res}}), \quad (2)$$

where $P_{\text{prior}}(m_{\text{res}})$ is the prior PDF for the reservoir parameters (including their spatial distributions) and $P_{\text{prior}}(m_{\text{elas}}|m_{\text{res}})$ is a conditional probability for the elastic parameters that summarizes the rock physics relationships between the reservoir property and elastic property. Thus, the final posterior PDF for the joint rock physics and seismic inversion is the following combination of Eqs. (1) and (2)

$$P_{\text{post}}(m_{\text{res}}, m_{\text{elas}}) = c P_{\text{prior}}(m_{\text{res}}) P_{\text{prior}}(m_{\text{elas}}|m_{\text{res}}) P_{\text{data}}(d_{\text{obs}} - g(m_{\text{elas}})). \quad (3)$$

The petrophysical conditional density $P_{\text{prior}}(m_{\text{elas}}|m_{\text{res}})$ is the rock physics forward function that maps the reservoir model parameters (lithofacies, porosity, and saturations) to the elastic model parameters. Many different seismic inversion work flows that combine elastic properties, geostatistics, and rock-physics models to predict reservoir properties can be presented in the shape of Eq. (3). This work flow in a Bayesian formulation guarantees consistency between the elastic and reservoir properties.

As shown by [Hansen et al. \(2012\)](#), the extended Metropolis algorithm samples the posterior PDF with the observed data and an assumed noise model. The likelihood of a given model is computed as

$$L(m_{\text{elas}}) = P_{\text{data}}(d_{\text{obs}} - g(m_{\text{elas}})) = \exp \left[-\frac{(d_{\text{obs}}^i - g^i(m_{\text{elas}}))^2}{2\sigma^2} \right], \quad (4)$$

where σ is the variance of the noise added to the synthetically forward-simulated data. Two different noise models for each different type of seismic data (i.e., acoustic impedance in depth and seismic section of seismograms in time) are applied. One of main sources of the noise in our example is the uncertainty in the rock physics models for the sand and shale facies. Since P-wave velocities and densities are not constant values but assigned from a bivariate PDF of each facies, the computed acoustic impedance has a large variability. For the impedance data, a frequency-domain Born filter is applied to consider surface seismic reflection geometry with a bandwidth from 5 to 50 Hz. The Born weak scattering approximation for the effect of image distortions and its applications have been widely studied by [Bleistein and Gray \(1985\)](#), [von Seggern \(1991\)](#), and [Mukerji et al. \(1997\)](#). For the normal-incidence seismic section, convolutional seismic forward modeling with 10% random noise and a 50 Hz wavelet are assumed and applied.

2.2 Rejection Sampling

Sampling the posterior models is more important than a single optimization result, but in practice it may be nearly impossible to apply because sampling takes tremendous time and cost. These problems are especially critical in complex models such as actual reservoir cases. Tarantola (2005) gave an overview of an exact method to obtain representative samples of $P_{\text{post}}(m|d)$. Rejection sampling is based on the fact that the posterior is a subset of the prior distribution, and; therefore, it can be evaluated by sampling the prior data. This approach consists of generating candidate models m^* that are samples of $P_{\text{prior}}(m)$ and accepting each of them with a probability in Eq. (5),

$$P(m^*) = \frac{L(m^*)}{L(m)_{\max}}, \quad (5)$$

where $L(m)$ is the likelihood which represents the misfit between the observed data (d_{obs}) and the forward-simulated model ($g(m)$). $L(m)_{\max}$ denotes the supremum, which can be any number equal to or above the maximum likelihood value that can be taken by $L(m)$. The distribution of the resulting samples follows a posterior distribution of the models. Since it requires a large number of evaluations of $P_{\text{prior}}(m)$, the rejection method is inefficient.

2.3 Iterative Spatial Resampling

The Metropolis algorithm (Metropolis et al. 1953) samples the posterior by forming a Markov chain of models, such that the steady-state distribution of the chain is precisely the posterior distribution that one wishes to sample from. It is similar to a random walk that would preferentially visit the areas where $P_{\text{post}}(m|d)$ is high (Hansen et al. 2008, 2012). In reservoir modeling, the specific issue is how to form and perturb a Markov chain while preserving the spatial structure of the geomodels in the chain. One way is to sample a subset of points from previous models in a chain, and use the points as conditioning data for the next simulated realization. Since the simulation uses the same training image (or other spatial information about the prior data), the spatial structure of the models in the chain is preserved.

Hansen et al. (2008) and Mariethoz et al. (2010a, b) suggested this iterative spatial resampling (ISR) method, which perturbs the realizations of a spatially dependent variable while preserving its spatial structure. This method is used as a transition kernel to produce Markov chains of geostatistical realizations. It has been applied to flow problems but has not been tested for seismic inversion. Implementing the Metropolis sampler using ISR (M-ISR) to sample the prior is accomplished by performing the following steps at each iteration i (Figs. 2, 3). The detailed procedure of M-ISR is described in Algorithm 1.

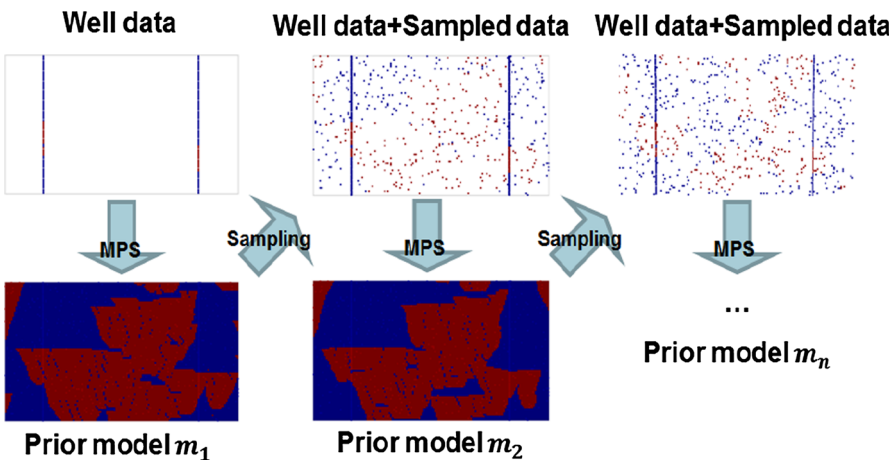


Fig. 2 A sketch of the iterative spatial resampling method (ISR); an initial model m_1 is randomly sampled to obtain the subset, which is used as conditioning data for generating the next model m_2 ; m_2 displays similar local features to m_1 due to the constraints imposed by the conditioning data, but represents a different realization from the prior multi-point geostatistical model

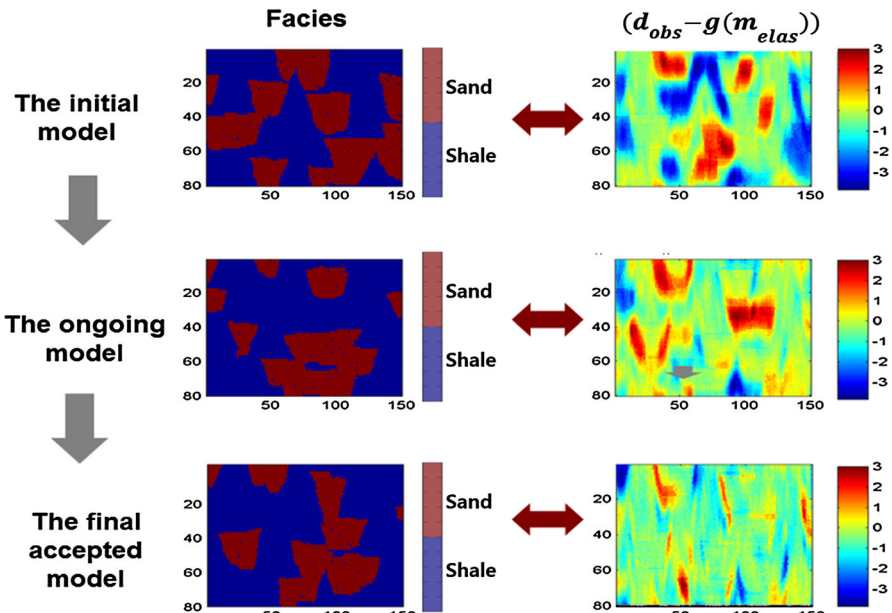


Fig. 3 The iteration of a Markov chain using ISR; generated facies models are shown in the left column, and the residual difference between the obtained acoustic impedance and the predicted acoustic impedance from the earth model in each step is displayed in the right column; this misfit gets smaller with iterations (acoustic impedance unit: MRayl = $10^6 \frac{\text{kg}}{\text{s m}^2}$)

Algorithm 1: Metropolis sampler using ISR (M-ISR)

Input: Training image, obtained seismic data, a number of subset points

Steps:

- a. Generate the first model m_1 by multi-point geostatistical simulation and evaluate its likelihood, $L(m_1) = P_{\text{data}}(d_{\text{obs}} - g(m_1, \text{elas}))$. The model of current state $m_c = m_1$.
- b. Select r_i as a random subset of points from m_c . Note that initial conditioning datasets such as core or well-log data are included in subset points for next model generation.
- c. Generate a proposal model m^* by conditional simulation using r_i as conditioning data.
- d. Evaluate $L(m^*)$ and accept m^* with probability,
 $P_{\text{accept}} = \min(1, L(m^*)/L(m_c))$ (Metropolis et al. 1953; Mosegaard and Tarantola 1995).
- e. If m^* is accepted $m_c = m^*$; else reuse m_c .
- f. Iterate b–e.

The Metropolis sampler using ISR theoretically samples the exact posterior distribution as an alternative method to a rejection sampler. However, in terms of efficiency, it is still slow and impractical. Thus, the authors propose a compromise to make it applicable by using auxiliary information. The price to pay is that the sampling is inexact, even though illustrated test cases show that in practice the sampling is often reasonably accurate.

2.4 Adaptive Spatial Resampling

The search strategy of ISR performs successive steps in random directions to explore various regions of the solution space. Since the search is stochastic, the posterior distribution will theoretically be reached after an infinite number of iterations. However, in most practical applications, when the subset conditioning points are selected at random, ISR can get stuck for a very long time in a non-optimal local minimum. In this work, the authors propose to improve the efficiency of ISR by utilizing adaptive sampling.

At every iteration, the predicted seismic data is compared with the observed data and thus a spatial error map is always computed. Figure 4 shows an example of the spatial error map; it is a residual error between a forward-simulated model and the obtained data. The proposed work flow uses this spatial information to generate the next step. Instead of randomly sampling a subset of points to condition the next realization, it adaptively samples important points having lower residual errors (see Fig. 4). The idea is to freeze for the next iteration parts of the domain that yield a low error, while the high-error locations can be updated. The algorithm probabilistically selects a subset of conditioning points, with a probability based on the residual error PDF. Locations with a lower error have a higher chance to be accepted as conditioning points. The probability of a location to be selected as conditioning data for the next iteration is defined as

$$P_{\text{cond}}(x) \propto \frac{N - R(x) + 1}{N} \quad \forall R(x) = \text{Rank}(|\text{error}(x)|), \quad (6)$$

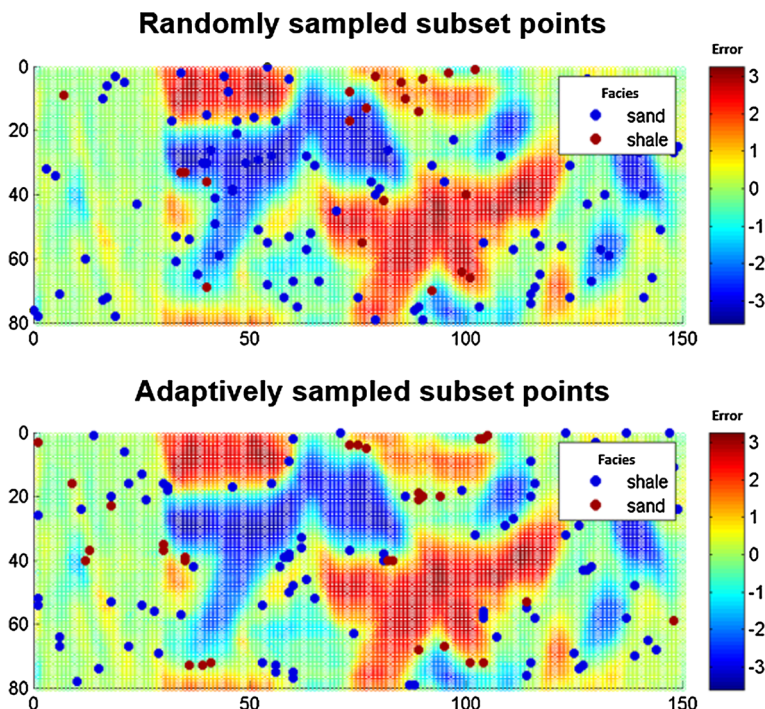


Fig. 4 The sampling algorithm of the subset points in ASR; the seismic attribute used here is the inverted seismic impedance; the *background green zone* is the low residual points while both *red* and *blue* have higher errors; in the residual error map, randomly sampled points (*top*, ISR) are located in both low and higher error zones, while the adaptive sampling subsets (*bottom*, ASR) are located preferentially in the low error zones

where $\text{error}(x)$ is the misfit at each cell location x and N is the total number of cells in an error map. The number of resampled points is defined as a fraction of the total number of cells. The Rank ($|\text{error}(x)|$) function returns N for the absolute maximum error and 1 for the absolute minimum error, respectively. Thus, the probability to be selected as a subset point is $1/N$ for the maximum error and 1 for the minimum error. Next, the algorithm visits a random point x and accepts the point if $P_{\text{cond}}(x)$ is higher than a uniform random number on a 0–1 scale. This preferential probabilistic selection of favorable locations causes Metropolis sampling with Adaptive spatial resampling (M-ASR) to accelerate the procedure and to efficiently sample posterior models consistent with the given data. The M-ASR procedure is explained in more detail in Algorithm 2.

The idea to use auxiliary values of a previous state with probabilistic preference is very similar to the adaptive McMC (Haario et al. 2001) and the auxiliary variable sampler (Andrieu et al. 2003). The adaptive McMC is a scheme to tune the proposal distribution using previous values of the chain. Since conventional Markov chains can get stuck in a certain state for a long time, updating the proposal distribution can help the chains reach the posterior distribution earlier. Many algorithms and examples have been discussed (e.g. Roberts and Rosenthal 2009; Andrieu and Thoms 2008), and

the proposed M-ASR algorithm is an analogous variant of the adaptive McMC and auxiliary variable sampler. However, the adaptive McMC may potentially violate the Markov property of the transition kernel. If it is not properly controlled, the results of seismic inverse modeling could be a biased sampling of the posterior distribution, since it does not fully honor the detailed balance. Theoretically, the chance to recover the original state is lower in the adaptive Markov chains than in the traditional ones. Thus, in the worst case, the results may seriously underestimate a range of uncertainty in the posteriors.

To avoid this problem, [Andrieu et al. \(2003\)](#) suggested using adaptation only during an initial fixed number of steps, and next doing pure McMC after jumping to the posterior distribution. This paper focuses on the applicability of the M-ASR as an approximate and alternative posterior sampler; however, one could carry out theoretically sound posterior sampling with both ASR for the burn-in period and ISR for the standard McMC simulation. The authors claim that the M-ASR is a fast and approximate sampling method, since it partially violates the detailed balance. To ensure exact sampling of the posterior distribution, a detailed balance is a necessary condition as the M-ISR follows. One interesting feature of M-ASR is that it behaves similarly to the M-ISR when they both reach a constant error map. M-ASR is only effective when the spatial error map has local variations; however, the error map evolves with iterations and then the M-ASR becomes close to a pure McMC. Thus, the closer spatial error map is to a constant, the closer the M-ASR algorithm is to ensuring a detailed balance. Therefore, the violation of detailed balance and its fruitful acceleration happens during the evolution periods. The recursive force to search a wide prior distribution still exists in the M-ASR, as in a classical McMC Metropolis sampler.

Algorithm 2: Approximate Metropolis sampler using ASR (M-ASR)

Input: Training image, obtained seismic data, a number of subset points

Steps:

- Generate the first model m_1 by multi-point geostatistical simulation and evaluate its likelihood, $L(m_1) = P_{\text{data}}(d_{\text{obs}} - g(m_1, \text{elas}))$. The model of current state $m_c = m_1$.
- Select r_i as an adaptive subset of points from m_c . Note that initial conditioning datasets such as core or well-log data are included in subset points for next model generation.

If the obtained seismic data is an inverted acoustic impedance in depth:

- Build a PDF of Eq. (6).
- Visit a random point x and accept the point if $P_{\text{cond}}(x) > a, \forall a \in U[0, 1]$.
- Iterate the above steps until the assigned number of subset points are found.

If the obtained seismic data is a seismic section of seismograms in time:

- Build a PDF of Eq. (7).
 - Visit a random Common Depth Point (CDP) x and accept random points in the CDP x if $P_{\text{cond}}(x) > a, \forall a \in U[0, 1]$.
 - Iterate the above steps until the assigned number of subset points are found.
 - Generate a proposal model m^* by conditional simulation using as r_i conditioning data.
 - Evaluate $L(m^*)$ and accept m^* with probability, $P_{\text{accept}} = \min(1, L(m^*)/L(m_c))$ ([Metropolis et al. 1953](#); [Mosegaard and Tarantola 1995](#)).
 - If m^* is accepted $m_c = m^*$; else reuse m_c .
 - Iterate b-e.
-

The adaptive selection algorithm should be modified depending on the type of seismic data. Inverted acoustic impedance data in depth can be compared with predicted data directly to calculate a residual error map, as shown in Fig. 4. This is because the simulated realizations of the earth models are also in depth, and the subset of points to condition the next model is required in depth. However, if the data are the stacked seismic traces recorded in time (before impedance inversion), a direct comparison between the data and a prediction can be misleading because of timeshifts. The two seismograms in Fig. 5 show similar local features at Common Depth Point (CDP) 20; however, since the seismic reflections do not exactly overlap in the time axis, the directly subtracted residual error is still high regardless of the similarity of the underlying facies. Thus, the authors propose using trace-to-trace cross-correlation coefficients to guide the probability of selection, as shown in Eq. (7). A higher correlation coefficient assigns a higher chance to be accepted as a conditioning location for the next step

$$P_{\text{cond}}(\mathbf{x}) = \text{Corr}(m(\mathbf{x}), d(\mathbf{x})), \quad (7)$$

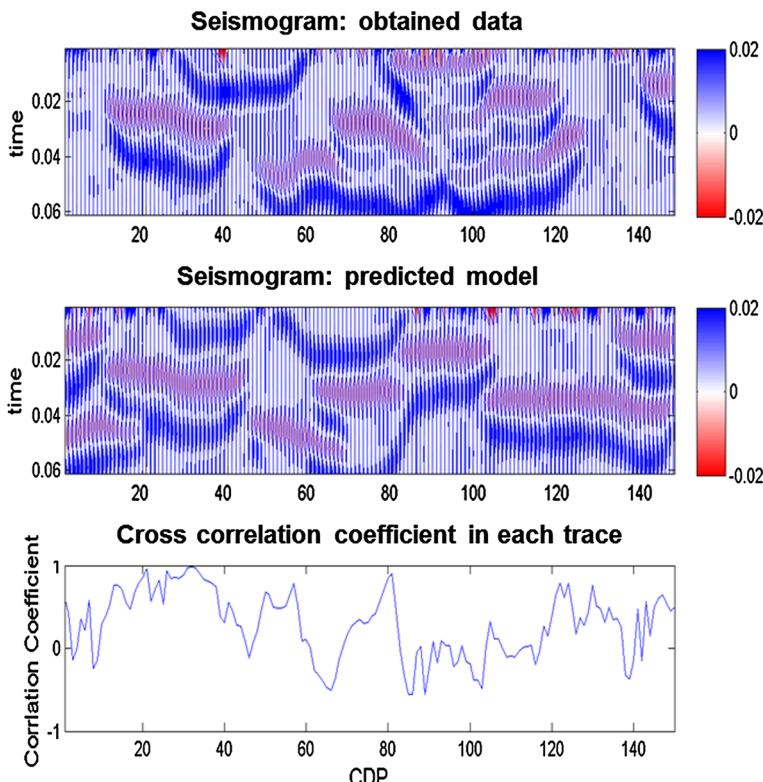


Fig. 5 The subset sampling algorithm for a seismogram in the ASR; since the seismogram has traces consisting of wiggles in travel time, directly subtracted variability can miss similar local features; the cross-correlation coefficients of each pairwise traces are used for adaptive sampling of subset points; the location of a trace having a high correlation coefficient with the corresponding data trace has a greater chance to be selected as a subset point for conditioning the next iteration in the chain

where $m(\mathbf{x})$ is a seismogram of the proposed model at line \mathbf{x} and $d(\mathbf{x})$ is a seismogram of data at line \mathbf{x} . Azevedo et al. (2012) suggested keeping the best parts of the proposed model based on correlations between the data and the synthetic model. However, here the authors propose a more probabilistic perturbation, using subset points from the higher correlation area rather than freezing the best parts for optimization.

Depending on the acceptance/rejection criterion in the Markov process, it is possible to obtain a chain of realizations intended to characterize a certain posterior distribution with Metropolis sampling. In the studied cases discussed below, an M-ASR (Approximate Metropolis sampler using ASR) yields posterior distributions reasonably close to the ones obtained by rejection sampling, but with an important reduction in CPU cost. Due to the directed resampling of points, ASR does not produce a reversible Markov chain and, therefore, is not an exact sampler. However, at every iterative step in the chain, ASR proposes a possible subset configuration which has more informative points for finding a better model more efficiently. The resampling process is performed probabilistically depending on the error PDF or cross-correlation coefficients. To gain practical efficiency, M-ASR can be a promising alternative sampling method for both the Metropolis sampler with ISR and the rejection sampler. The following illustrations demonstrate how the M-ASR efficiently approximates the posterior distribution while keeping a similar range of uncertainty as a rejection sampler.

3 Application

3.1 Two-Dimensional Vertical Section Examples

Synthetic two-dimensional facies and a seismic dataset are presented to demonstrate the validity of the proposed inversion technique. The reference model and corresponding seismic data were extracted from a modified version of the top layer of the Stanford VI synthetic reservoir (Castro et al. 2005). All the information about the model relevant to this work is summarized in Fig. 6. The reference facies model is a sand-shale channel system with 80 cells in the vertical (z) direction ($d_z = 1$ m) and 150 cells in the horizontal (x) direction ($d_x = 25$ m).

First, multiple prior spatial models are generated by using a MPS algorithm (direct sampling); these are used to find posterior models by rejection sampling. The rejection sampling method is one way to represent the posterior PDF. Each accepted model in the rejection sampler is by definition a realization of the posterior distribution. Figure 7 shows the results as the reference and the E-types (ensemble averages) of the models. Note that the displayed probability of ensemble averages demonstrates the distribution of sand facies. Since the hard data come from two wells, the E-type map of priors shows its limitation in terms of lateral resolution. Rejection sampling is performed to represent posterior PDF as the reference. The authors tested the M-ISR as an equivalent sampling method and the M-ASR as a fast approximation by comparing their results with the rejection sampler. The following sections introduce a sensitivity analysis of the M-ASR parameters and three different two-dimension case studies. The authors demonstrate the use of M-ASR for two types of seismic data and a particular case for identifying a different reservoir fluid not encountered in the well

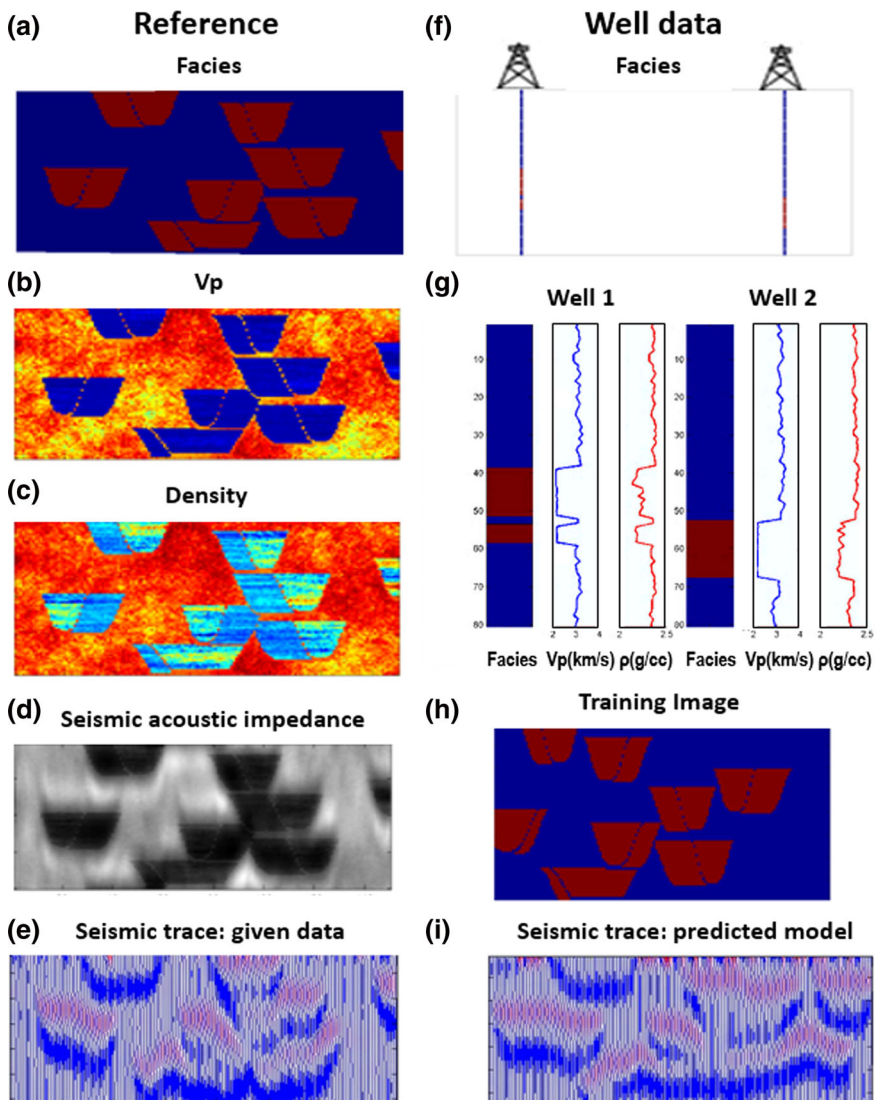


Fig. 6 A summary of a sample two-dimensional vertical section; **a** the spatial distribution of the facies, **b** P-wave velocities (V_p), **c** densities (ρ), **d** the filtered seismic band acoustic impedance, and **e** normal-incidence seismograms as reference; Other images: **f** two wells at CDP 25 and CDP 125, **g** its logging data, and **h** a training image for MPS are available as given data; The predicted model in data space **i** is compared to the given data **e** in the inversion process

data. Case study 1 is where P-impedance inverted from the seismic section is available, and the impedance data is used as an attribute for the stochastic lithofacies inversion. In case study 2, the seismic data are the normal-incidence seismograms themselves, before inversion for impedance. Case study 3 is where one tries to identify a different reservoir fluid not encountered in wells by applying Gassmann's equation (Avseth

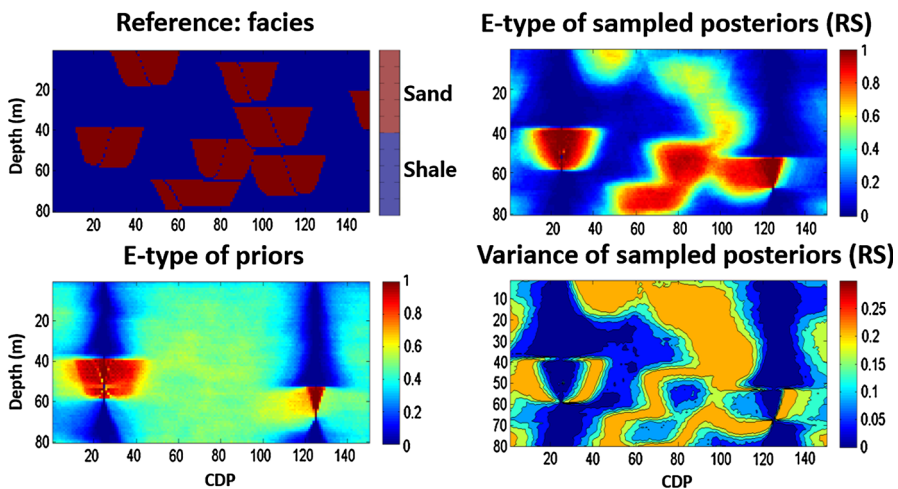


Fig. 7 A representation of the averages of the models' ensembles; the reference facies and the ensemble averages of prior models are shown in the *left* column; the ensemble averages of the rejection sampling results and its variance are displayed in the *right* column

et al. 2005). Gassmann's equations enable one to calculate seismic velocity changes according to a fluid substitution. From the given set of velocity V_p , V_s , and density, one can compute the changes in the reservoir with another set of fluid. This case study explores a what-if scenario assuming the existence of a different reservoir fluid, as a possible application of seismic inverse modeling.

3.1.1 Sensitivity of Parameters

As shown in Mariethoz et al. (2010a, b), the performance of M-ISR could be sensitive to changes in input parameters. Since M-ASR follows a similar work flow to M-ISR except for the preferential subset sampling, essentially M-ASR is also sensitive to input parameters such as the fraction of selected conditioning points and the number of trace locations in a seismogram section. The fraction of subset points controls iteration steps for searching out the next better model. A large fraction of conditioning points makes too little progress at every iteration step, while a small fraction can move in relatively large steps but may lose the local features of the previous model. The optimal fraction varies depending on the problems. The authors tested the sensitivity to this parameter and found that adaptive resampling with a 1% proportion performs slightly better than the other values in the illustrated case (left side, Fig. 8). In this figure, it is observed that retaining a large fraction rapidly reduces the root mean square error (RMSE) at the beginning, but it gets stuck in a local minimum after 100 iterations. In contrast, chains with a 1% fraction move relatively slower but can reach a lower RMSE. Note that the fraction rate does not count the initial conditioning data at the well locations. The number of selected traces is also an important parameter for the seismic section data of seismograms. More traces account for more horizontal spatial structures, while it may lose vertical information in the seismic trace since fewer points are selected

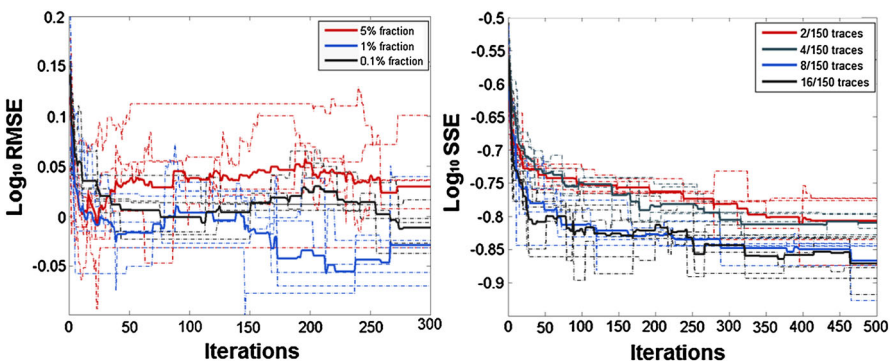


Fig. 8 Performance assessment for testing different parameters; the *dotted lines* are each Markov chain and the *thick line* is the average of five different chains; the *left figure* shows the sensitivity of the fraction rate of subset points tested in a two-dimensional acoustic impedance case; the error is recorded in logarithmic root mean squared error (RMSE); adaptive resampling with a 1% fraction of conditioning subset points performs slightly better than the other values, but this can be different depending on the problem; the *right figure* shows the sensitivity of the number of traces tested in a two-dimensional seismic section case; the total error is displayed by the logarithmic summation of squared error (SSE) at each CDP line, since the comparison of each vertical trace is more suitable for the seismogram than pixel-wise error computation; the eight traces case was an ideal setting in this study

per trace. In the illustration case (right side, Fig. 8), the number of traces affects the efficiency of the Markov chain while the fraction rate is fixed at 1%. The sensitivity test within our dataset shows eight trace locations with a 1% fraction rate are relatively suitable in this case.

3.1.2 Case Study 1: Two-Dimensional Acoustic Impedance Inversion

For the impedance inversion process, it is assumed that only the two-dimension acoustic impedance data (shown in Fig. 6d) as the obtained seismic data, two wells with log information, and a training image are available. Based on the relationship between facies (reservoir property) and P-wave velocity and density (elastic properties) from the well data, Monte-Carlo simulation is performed to build a statistical rock physics model as a bivariate PDF. Using the statistical rock physics model for the sand and shale, acoustic impedances are calculated from the P-wave velocities and densities. Computation of the inverted seismic impedance is done by applying a frequency-domain Born filter for surface seismic reflection geometry, with a bandwidth from 5 to 50 Hz.

When acoustic impedance data is used as the seismic attribute, both the rejection sampler and M-ASR found clear channel distributions. These results look the same, while M-ISR found a similar channel distribution with some ambiguity (first row of Fig. 9). However, the result of the rejection sampler is the average of 125 accepted models after evaluating 100,000 prior models, while the ASR with Metropolis algorithm uses five Markov chains with 1000 iterations (146 posterior models sampled in M-ASR and 28 posterior models sampled in ISR). M-ASR shows a significantly lower rejection rate compared to ISR. The RMSEs versus iterations for five Markov chains

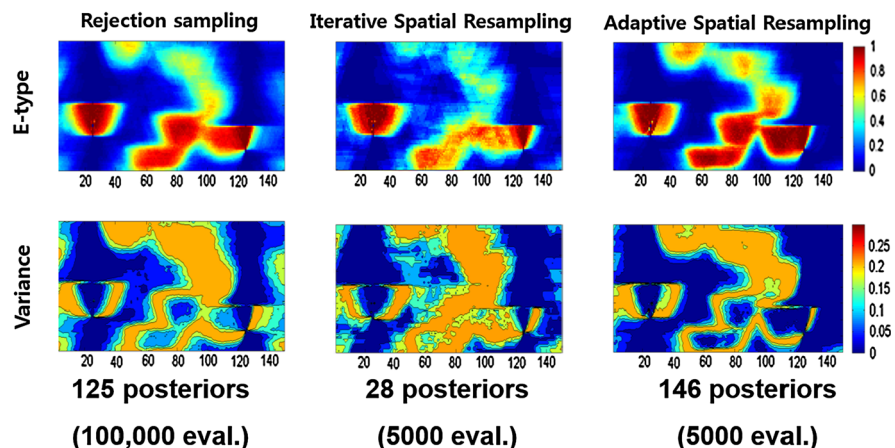
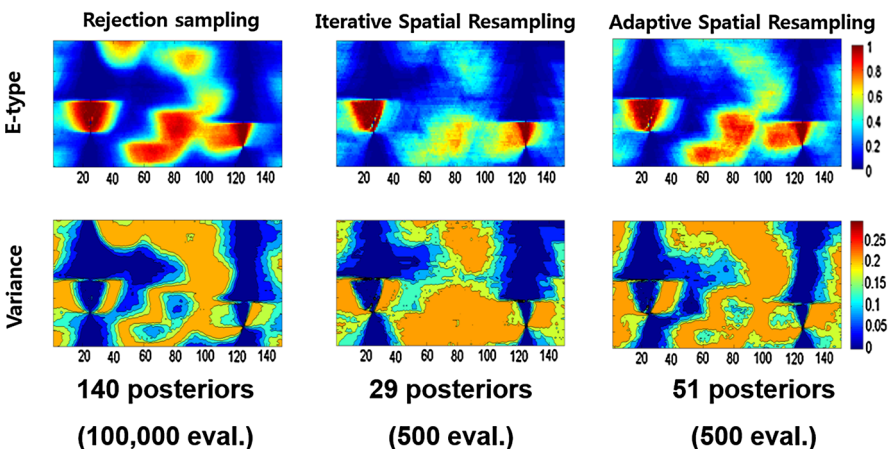
1. Acoustic impedance**2. Seismogram**

Fig. 9 A representation of the averages of the models' ensembles; *first row* the E-type of rejection sampling results, M-ISR, and M-ASR, using acoustic impedance as the observed seismic attribute; *second row* the respective variance of each algorithm; *third and fourth rows* the E-type of the rejection sampler, M-ISR, and M-ASR using a seismogram section as the obtained data and its variance (*fourth row*); M-ASR shows similar E-type and variance maps compared with the result of rejection sampling in both cases, within the limited evaluations

are shown in Fig. 10, comparing the behavior of M-ISR and M-ASR. The M-ASR chains reached a lower error zone more rapidly than the ISR chains, yielding more samples for the same number of iterations.

The M-ISR chains also converge in the low error zone but take a longer time than M-ASR. The M-ASR chains move up and down rapidly and hit more lower error models compared to M-ISR. Thus, the averaged chain of M-ASR moves around the relatively lower error region more than the averaged M-ISR chain in Fig. 10 (thick lines). However, the sampled posterior models from the M-ISR and M-ASR chains of

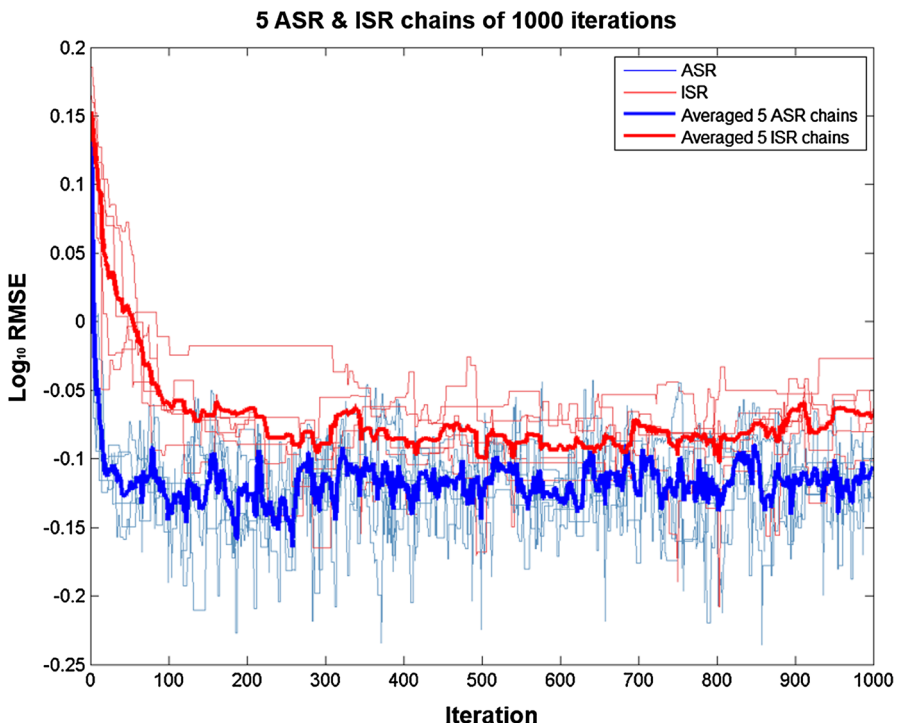


Fig. 10 A comparison of Markov chains formed by adaptive spatial resampling (in blue) and iterative spatial resampling (in red); the average of five chains is shown as a thick line; ASR chains rapidly reach the lower error zone

Fig. 10 shows very similar distributions of RMSEs in Fig. 11. The posterior samples are accepted after the burn-in period of ISR (100 iterations later). Sampling is performed at least ten iterations later from the previous sample, but not performed when the chain gets stuck in a certain state. The histogram of M-ISR is distributed in a slightly higher RMS error zone than M-ASR; however, both distributions are nearly overlapping and the median values are almost the same.

3.1.3 Case Study 2: Two-Dimensional Seismograms Inversion

To generate a reference normal-incidence seismic section, convolutional seismic forward modeling with 10% white noise is applied with a 50 (Hz) wavelet. For the inversion process, the authors assumed that the seismogram section, two wells with log information, and a training image (shown in Fig. 6e, g, h, respectively) are available for the seismic inversion. At every iteration, the generated facies model is forward-simulated to predict the corresponding two-dimensional seismic section, as shown in Fig. 6i. Next, the difference is estimated between the predicted seismic responses and the obtained data.

Since seismogram data have more uncertainty than acoustic impedance due to the wavelet effect and time shifts, the predictability of the sampling algorithm is critical in

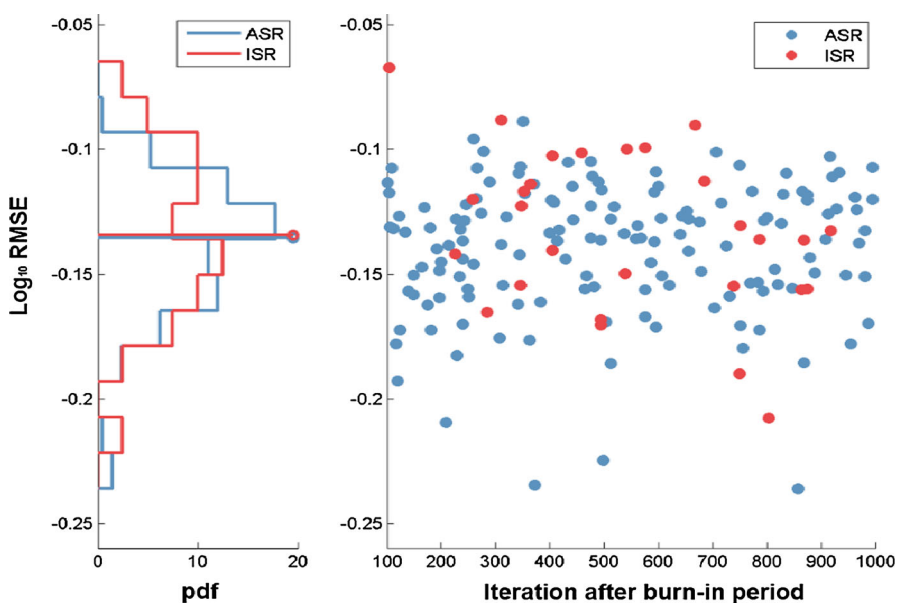


Fig. 11 A comparison between the sampled posteriors of M-ISR and M-ASR; after the burn-in period of the ISR chain, posteriors are sampled from five M-ISR (red dots) and M-ASR (blue dots) chains, respectively; each distribution of samples is shown in the *left* histogram; the distribution of M-ISR is slightly higher than the M-ASR, but the two distributions nearly overlap and the median values are almost the same

this case. The performance of M-ISR and M-ASR are compared in the bottom of Fig. 9, which shows a large difference in the E-type result. M-ASR found a similar spatial distribution of channels as the rejection sampler did, while M-ISR lost channels away from the wells (ISR sampled 25 posterior models in a chain). The M-ASR sampled 51 posterior models in one Markov chain with 500 iterations, while the rejection sampler accepted 140 posterior models among 100,000 priors. A variance map (the bottom figures in each section of Fig. 9) shows that M-ASR captures the range of uncertainty fairly well compared with the rejection sampler. To visualize the distribution of priors and the similarity of posterior samples which come from the different methods, the results are projected in a multi-dimensional scaling (MDS) map (Scheidt and Caers 2009). The distance-based representation using MDS in Fig. 12 illustrates that the samples from M-ASR are distributed near the reference with the posterior models from the rejection sampling. Thus, the authors conclude that the M-ASR is in this case a fair approximation of a rejection sampler. Since our reference is located away from most of the prior models, the rejection sampler is inefficient to find the posterior models. The posterior models sampled by M-ISR could not yet reach the whole posterior distribution, due to the limited iterations. In contrast, the similarity of the averaged ensemble map and variance between the rejection sampler and the M-ASR shows that the M-ASR rapidly samples the posterior distribution approximately within the limited number of iterations.

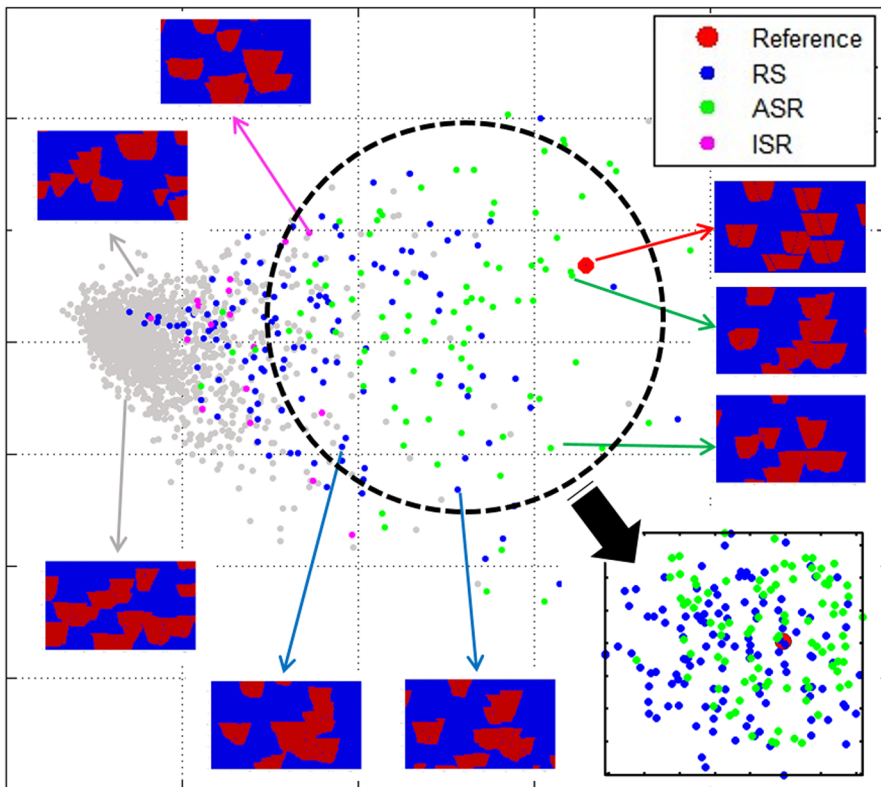


Fig. 12 A multi-dimensional scaling (MDS) projection of all models using a Euclidean pixel-wise distance: the reference (in red), prior models (in gray), the posterior samples by rejection sampling (in blue), M-ASR (in green), and M-ISR (in magenta)

3.1.4 Case Study 3: Identifying a Facies Not Observed in Wells

In this case, the authors assume one oil sand distribution away from the two wells' locations. In this example, a two-dimensional seismic section of seismograms, well-logs without oil sand information, and a training image are available. For this task, a realistic rock physics relationship from actual well-logs is applied, and oil sand properties are generated from the brine sand properties at the wells by using Gassmann's equation (see Fig. 13c). Figure 13d, e shows the rejection sampler and the M-ASR results as probability maps. The rejection sampler found a spatial distribution of facies close to the reference after 50,000 evaluations, while M-ASR found a similar distribution using one chain of 1000 evaluations. In this more realistic setting, M-ASR also shows its applicability. The reduction of the total number of evaluations becomes more meaningful as the model gets larger and more realistic (i.e., complex and high-dimensional). In the following example of a three-dimensional case, a rejection sampler is nearly impossible since it requires an extremely long time to sample a posterior distribution. Roughly, if the sampler needs 50 times more evaluations to sample similar posteriors

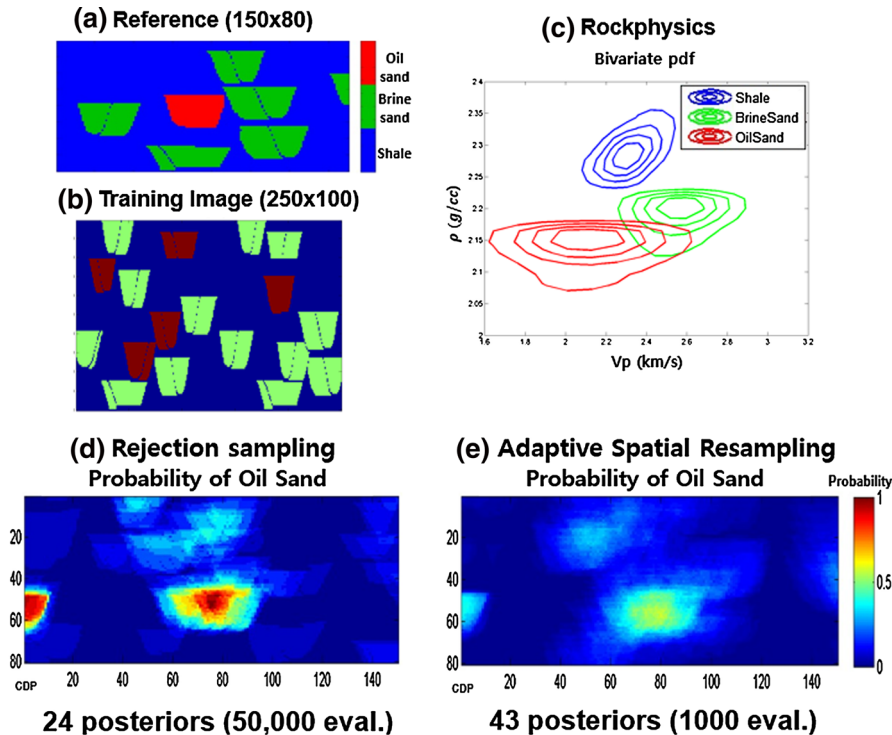


Fig. 13 A case study for detecting oil sand distribution away from wells when the wells do not have any oil sand: **a** the three reference facies, **b** a training image, **c** a bivariate PDF of each facies as a rock physics model, **d** the probability maps for oil sand facies obtained from the rejection sampler, and **e** the probability maps of the oil sand facies obtained from the posterior models sampled by M-ASR; the probability of oil sand is projected as a representation of the averages of ensembles of oil sand in the sampled posteriors; M-ASR shows a similar probability map compared to the result of the rejection sampler within a relatively limited number of evaluations

based on this case study result, arithmetically it would take 20 days for modeling, which is not acceptable in general (compared to the case of M-ASR using SNESIM, in Table 1).

3.2 Application to a Three-Dimensional Seismic Inversion

3.2.1 Introduction to the Studied Three-Dimensional Case

As discussed in Sect. 1, seismic inverse modeling can be classified into two groups: the sequential approach, and the simultaneous work flow in a Bayesian formulation. In this illustration case, the authors extend the proposed approach to the three-dimensional case, and the result is compared to a sequential approach, using seismic data as soft-data to condition for geostatistical simulation. The proposed approach generally takes a longer time because the seismic data is used only for falsifying models, not for generating models. However, this approach accounts for the elastic parameters and the

Table 1 Comparison of input and output between the proposed inversion and the sequential inversion

	Proposed inversion	Sequential inversion
MPS parameters	No. of nodes in search template: 60 Range: max 50/med 50/min 20 Angle: Azimuth 0/Dip 0/Rake 0	
Total evaluations for generating 20 samples 2 chains (40 for burn-in) 280 evaluations 20 models		
Computation time using SNESIM	10 h ^a	3 h ^a
Computation time using DS	3 h ^a	

^a A computer setting of 3.3 GHz (4 CPUs) and 16 GB RAM

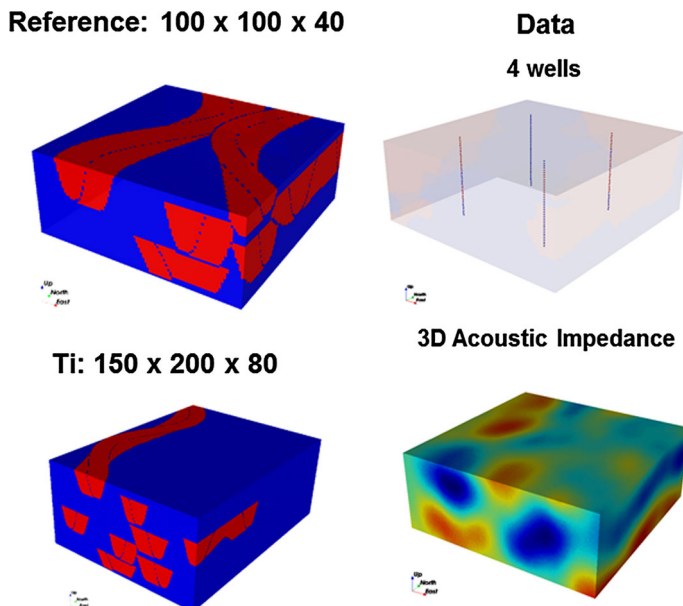


Fig. 14 A three-dimensional case study for comparing a sequential inversion approach with the proposed simultaneous inversion; the reference of sand and shale facies and a training image used for this case are shown in the *left* column; four wells and an acoustic impedance cube as seismic data are assumed as the obtained data

reservoir properties together in a Bayesian formulation, so it can improve the consistency between properties. Also, the obtained spatial data does not directly influence the prior generation. The problem setting of the three-dimensional case is shown in Fig. 14. The reference field is a set of partially stacked sand channels. The only available data is four wells located at the (25, 25), (25, 75), (75, 25), and (75, 75) grid-points, respectively, and a three-dimensional acoustic impedance cube as seismic data. It is assumed that the given training image (shown in the bottom-left corner of Fig. 14) successfully captures the spatial continuity of the reference case. In a real field, the selection of a training image is a crucial task for successful reservoir modeling. Ways

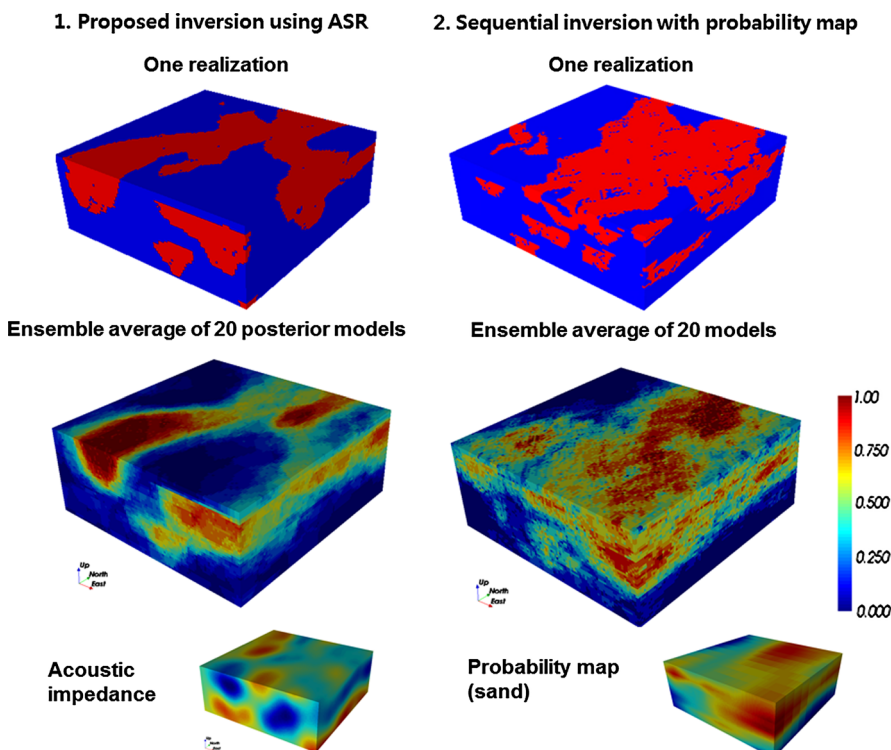


Fig. 15 A result of the three-dimensional case study; a set of the results of the proposed simultaneous inversion using Metropolis ASR are shown as (top) a sampled posterior, (middle) the averaged E-type map of 20 posterior models, and (bottom) the given acoustic impedance; a set of the results of the sequential inversion using soft data are displayed as (top) a sampled posterior, (middle) the averaged E-type map of 20 posterior models, and (bottom) the sand probability map used as soft data for the geostatistical simulation

to identify valid training images as the most likely geological scenarios are studied by [Jeong \(2014\)](#) and [Scheidt et al. \(2015\)](#).

3.2.2 Three-Dimensional Seismic Inversion of a Simultaneous Approach and a Sequential Approach

The sequential approach firstly transforms the obtained acoustic impedance into a probability map, then conditions it as soft data in the geostatistical simulation. The transformed probability map of sand facies is displayed at the bottom right of Fig. 15, and is generated by Bayes' rule as given in [Castro et al. \(2005\)](#). All the MPS input parameters are the same in both cases (Table 1), so the perturbation of MPS simulation is equivalently maintained.

The goal of three-dimensional seismic inversion is to generate 20 final models from each approach. For the proposed approach as a simultaneous inversion, two parallel chains sample ten posterior models from each chain after the burn-in period. Note that the parallelization of two chains was enough for this example case, since this case

study targeted only 20 samples. However, depending on the problem scale, the length of the burn-in period and the number of parallel chains would vary. The result of each single realization in Fig. 15 shows a distinctive difference in terms of the reproduction of geological similarity in the given training image. Since seismic data is not used as conditioning data for model generation in the proposed work flow, it keeps the geological features of the training image (i.e., the size of the geobody, continuity, etc.) in all prior models. In contrast, the realization of the sequential approach is strongly influenced by the probability map, and; thus, it may lose some geological information in the training image. Compared to the reference, the averaged E-type map of the proposed work flow shows more similar and clearer sand channels distribution than the results of the sequential inversion. As shown in Table 1, the total computational time of M-ASR using DS is similar to the sequential inversion result, even though the total number of evaluations has a big difference. Since the time consumption is mostly caused by MPS simulation, newly proposed MPS algorithms such as DISPAT ([Honarkah and Caers 2012](#)) and CCSIM ([Tahmasebi et al. 2012](#)) may help to speed up the process, and enhance the applicability of M-ASR as a fast and geologically feasible seismic inverse modeling method.

4 Conclusions

In this paper, the authors presented approximate Metropolis sampling using an adaptive spatial resampling method (M-ASR) for fast seismic inverse modeling, which is an improvement of the M-ISR method. ASR perturbs the realizations of a spatially dependent variable while preserving its spatial structure. Compared to ISR, ASR accelerates the sampling efficiency since it uses the residual error at each step of the chain to guide the selection of conditioning data for the next step in a Markov chain. As shown in Fig. 12, MDS plots demonstrate that both the rejection sampler and M-ASR have a similar distribution of posterior samples, with M-ASR showing a slight reduction in the spread. In the studied cases, M-ASR yields posterior distributions reasonably close to the ones obtained by the rejection sampler, with an important reduction in time and computing cost. Thus, M-ASR appears to be suitable for reservoir characterization by conditioning facies models to spatially distributed seismic data.

Depending on the acceptance/rejection criterion in the Markov process, it is possible to obtain a chain of realizations intended to characterize a certain posterior distribution with Metropolis sampling. As a fast approximate sampler, ASR with Metropolis sampling is applicable in complex three-dimensional seismic inversions, which require a large number of iterations. The applicability of M-ASR will be improved if the MPS algorithm is more powerful for generating the reservoir models in each step. In the three-dimensional example case, most of the computation time consisted of MPS model generation since the size of the grid was 400,000 voxels. Reducing the number of evaluations for seismic inverse modeling increases the applicability in actual field cases.

This study will be applied to actual field data as a future task. The proposed work flow has used MPS as the geostatistical perturbation. However, it could be compared with any perturbation techniques, such as sequential Gaussian simulation or sequen-

tial indicator simulation. Also, the proposed work flow may be applicable to other sources of spatial data, such as inverted Controlled-source electromagnetic (CSEM) data, inverted resistivity sections, or Ground penetrating radar (GPR) data, and to other resources such as aquifer characterization.

Acknowledgements This research was funded by Stanford Center for Reservoir Forecasting (SCRF) sponsors.

References

- Andrieu C, Thoms J (2008) A tutorial on adaptive MCMC. *Stat Comput* 18:343–373
- Andrieu C, Freitas ND, Doucet A, Jordan MI (2003) An introduction to MCMC for machine learning. *Mach Learn* 50:5–43
- Arpat BG (2005) Sequential simulation with patterns. Dissertation, Stanford University
- Avseth P, Mukerji T, Mavko G (2005) Quantitative seismic interpretation. Cambridge University Press, Cambridge
- Azevedo L, Nunes RF, Almeida JA, Pinheiro LM, Caeiro MH, Correia PJ, Soares A (2012) Seismic attributes for constraining geostatistical seismic inversion. In: 9th International geostatistics congress, June 11–15, 2012, Oslo, Norway
- Bachrach R (2006) Joint estimation of porosity and saturation using stochastic rock-physics modeling. *Geophysics* 71(5):O53–O63. doi:[10.1190/1.2235991](https://doi.org/10.1190/1.2235991)
- Bleistein N, Gray SH (1985) An extension of the Born inversion procedure to depth dependent velocity profiles. *Geophys Prosp* 33(7):999–1022
- Bosch M, Cara L, Rodrigues J, Navarro A, Diaz M (2004) The optimization approach to lithological tomography: combining seismic data and petrophysics for porosity prediction. *Geophysics* 69:1272–1282
- Bosch M (1999) Lithologic tomography: from plural geophysical data to lithology estimation. *J Geophys Res* 104:749–766
- Bosch M, Mukerji T, Gonzalez EF (2010) Seismic inversion for reservoir properties combining statistical rock physics and geostatistics: a review. *Geophysics* 75(5):165–176
- Castro S, Caers J, Mukerji T (2005) The Stanford VI reservoir. 18th annual report, Stanford Center for Reservoir Forecasting, Stanford University
- Contreras A, Torres-Verdin C, Chesters W, Kvien K, Fasnacht T (2005) Joint stochastic inversion of 3D pre-stack seismic data and well logs for high-resolution reservoir characterization and petrophysical modeling: application to deepwater hydrocarbon reservoirs in the central Gulf of Mexico. In: 75th annual international meeting, SEG expanded abstracts, pp 1343–1346
- Doyen PM (2007) Seismic reservoir characterization: an earth modeling perspective. EAGE Publications, Houten
- Dubrule O (2003) Geostatistics for seismic data integration in earth models. SEG Publications, Tulsa
- Eidsvik J, Avseth P, Omre H, Mukerji T, Mavko G (2004) Stochastic reservoir characterization using prestack seismic data. *Geophysics* 69:978–993. doi:[10.1190/1.1778241](https://doi.org/10.1190/1.1778241)
- Gonzalez EF, Mukerji T, Mavko G (2008) Seismic inversion combining rock physics and multiple-point geostatistics. *Geophysics* 73(1):R11–R21
- Griffin JE, Walker SG (2013) On adaptive Metropolis–Hastings methods. *Stat Comput* 23:123–134. doi:[10.1007/s11222-011-9296-2](https://doi.org/10.1007/s11222-011-9296-2)
- Haario H, Saksman E, Tamminen J (2001) An adaptive Metropolis algorithm. *Bernoulli* 7:223–242
- Hansen TM, Mosegaard K, Cordua KC (2008) Using geostatistics to describe complex a priori information for inverse problems. In: Proceedings from VIII international geostatistics congress, vol 1, pp 329–338
- Hansen TM, Cordua KC, Mosegaard K (2012) Inverse problems with non-trivial priors—efficient solution through sequential gibbs sampling. *Comput Geosci* 16(3):593–611
- Honarkah M, Caers J (2012) Direct pattern-based simulation of non-stationary geostatistical models. *Math Geosci* 44(6):651–672
- Jeong C (2014) Quantitative reservoir characterization integrating seismic data and geological scenario uncertainty. Dissertation, Stanford University

- Larsen AL, Ulvmoen M, Omre H, Buland A (2006) Bayesian lithology/fluid prediction and simulation on the basis of a Markov-chain prior model. *Geophysics* 71(5):R69–R78. doi:[10.1190/1.2245469](https://doi.org/10.1190/1.2245469)
- Mariethoz G, Renard P, Straubhaar J (2010a) The direct sampling method to perform multiple-points geostatistical simulations. *Water Resour Res* 46:W11536
- Mariethoz G, Renard P, Caers J (2010b) Bayesian inverse problem and optimization with iterative spatial resampling. *Water Resour Res* 46:W11530
- Metropolis N, Rosenbluth AW, Rosenbluth MN, Teller AH, Teller E (1953) Equation of state calculations by fast computing machines. *J Chem Phys* 21:1087–1092
- Mosegaard K, Tarantola A (1995) Monte Carlo sampling of solutions to inverse problems. *J Geophys Res* 100(B7):12431–12447
- Mukerji T, Avseth P, Mavko G, Takahashi I, Gonzalez EF (2001a) Statistical rock physics: combining rock physics, information theory, and geostatistics to reduce uncertainty in seismic reservoir characterization. *Lead Edge* 20(3):313–319
- Mukerji T, Jorstad A, Avseth P, Mavko G, Granli JR (2001b) Mapping lithofacies and pore-fluid probabilities in a North Sea reservoir: seismic inversions and statistical rock physics. *Geophysics* 66:988–1001
- Mukerji T, Mavko G, Rio P (1997) Scales of reservoir heterogeneities and impact of seismic resolution on geostatistical integration. *Math Geol* 29(7):933–950
- Roberts GO, Rosenthal JS (2009) Examples of adaptive MCMC. *J Comput Graph Stat* 18:349–367
- Scheidt C, Caers J (2009) Representing spatial uncertainty using distances and kernels. *Math Geosci* 41(4):397–419
- Scheidt C, Jeong C, Mukerji T, Caers J (2015) Probabilistic falsification of prior geologic uncertainty with seismic amplitude data: application to a turbidite reservoir case. *Geophysics* 80(5):M89–M12. doi:[10.1190/geo2015-0084.1](https://doi.org/10.1190/geo2015-0084.1)
- Strebelle SB, Journel AG (2001) Reservoir modeling using multiple point statistics. In: SPE 71324 presented at the 2001 SPE annual technical conference and exhibition, New Orleans, 30 September–3 October 2001
- Tahmasebi P, Hezarkhani A, Sahimi M (2012) Multiple-point geostatistical modeling based on the cross-correlation functions. *Comput Geosci* 16:779–797. doi:[10.1007/s10596-012-9287-1](https://doi.org/10.1007/s10596-012-9287-1)
- Tarantola A (1987) Inverse problem theory: methods for data fitting and model parameter estimation. Elsevier, Amsterdam
- Tarantola A (2005) Inverse problem theory and methods for model parameter estimation. SIAM, Philadelphia
- Ulvmoen M, Omre H (2010) Improved resolution in Bayesian lithology/fluid inversion from prestack seismic data and well observations: part 1—methodology. *Geophysics* 75(2):R21–R35
- von Seggern DH (1991) Spatial resolution of acoustic imaging with the Born approximation. *Geophysics* 56(8):1185–1202